Fragility and hysteretic creep in frictional granular jamming

M. M. Bandi,[1,2,*] M. K. Rivera,[3] F. Krzakala,[2,4] and R. E. Ecke[2]
[1]*MPA-10, Los Alamos National Laboratory, Los Alamos, New Mexico 87545, USA*
[2]*T-CNLS, Los Alamos, National Laboratory, Los Alamos, New Mexico 87545, USA*
[3]*D-4, Los Alamos National Laboratory, Los Alamos, New Mexico 87545, USA*
[4]*CNRS and ESPCI ParisTech, 10 rue Vauquelin, UMR 7083 Gulliver, Paris 75000, France*
(Received 15 July 2012; revised manuscript received 11 February 2013; published 18 April 2013)

The granular jamming transition is experimentally investigated in a two-dimensional system of frictional, bidispersed disks subject to quasistatic, uniaxial compression without vibrational disturbances (zero granular temperature). Three primary results are presented in this experimental study. First, using disks with different static friction coefficients (μ), we experimentally verify numerical results that predict jamming onset at progressively lower packing fractions with increasing friction. Second, we show that the first compression cycle measurably differs from subsequent cycles. The first cycle is *fragile*—a metastable configuration with simultaneous jammed and unjammed clusters—over a small packing fraction interval ($\phi_1 < \phi < \phi_2$) and exhibits simultaneous exponential rise in pressure and exponential decrease in disk displacements over the same packing fraction interval. This fragile behavior is explained through a percolation mechanism of stressed contacts where cluster growth exhibits spatial correlation with disk displacements and contributes to recent results emphasizing fragility in frictional jamming. Control experiments show that the fragile state results from the experimental incompatibility between the requirements for zero friction and zero granular temperature. Measurements with several disk materials of varying elastic moduli E and friction coefficients μ show that friction directly controls the start of the fragile state but indirectly controls the exponential pressure rise. Finally, under repetitive loading (compression) and unloading (decompression), we find the system exhibits pressure hysteresis, and the critical packing fraction ϕ_c increases slowly with repetition number. This friction-induced hysteretic creep is interpreted as the granular pack's evolution from a metastable to an eventual structurally stable configuration. It is shown to depend on the quasistatic step size $\Delta\phi$, which provides the only perturbative mechanism in the experimental protocol, and the friction coefficient μ, which acts to stabilize the pack.

DOI: 10.1103/PhysRevE.87.042205 PACS number(s): 45.70.−n

I. INTRODUCTION

The "jamming" framework [1] has been proposed as an overarching, unifying description governing the behavior of a wide variety of disordered materials, including glasses, colloids, foams, and granular media via the jamming phase diagram with three axes representing temperature T, shear stress Σ, and inverse packing fraction $1/\phi$. Of particular interest is a point J at zero temperature and zero shear stress along the inverse packing fraction axis ($1/\phi$) predicted to have special properties. This point J is the critical packing fraction ϕ_c at which a frictionless granular pack undergoes a *sharp* transition from an athermal, particulate gas to a stiff, disordered solid. Numerics [2], mean-field theories [3,4], and experiments [5] all show that many interesting properties arise at this transition.

Being amenable to theoretical treatment, several early studies concentrated on idealized systems composed of *frictionless particles* and have contributed to the understanding of granular jamming. A growing body of numerical [6–10] and experimental [11–13] studies, however, conclusively demonstrate that interparticle friction substantially alters jamming behavior. Friction plays a significant role in granular materials: not only is it technologically relevant (e.g., in compression and sintering of ceramics [14]), but friction also radically alters the mechanical behavior of materials (e.g., in sedimentary rocks [15]). Understanding the role of friction in granular jamming therefore becomes relevant and important.

This article, which contributes to this growing body of results, presents an experimental study of frictional granular jamming of a loose, granular pack comprising a two-dimensional, bidisperse system of disks subjected to quasistatic, uniaxial compression (loading) and decompression (unloading). The following experimental results and their interpretations are presented.

(i) By employing disks with different static friction coefficients, we verify numerical predictions [7,16] for the effect of friction on the onset of jamming.

(ii) We show that the pressure scaling differs remarkably between the first and subsequent loading cycles. In the first cycle, as the system's boundaries are moved in to achieve an increasingly tighter packing, a fragile state is observed where the pressure exhibits an exponential rise $P \propto e^{\phi/\chi_P}$ over a range of packing fractions ($\phi_1 < \phi < \phi_2$), followed by a deviation from exponential scaling for $\phi > \phi_2$. This exponential rise in pressure is simultaneously reflected in an exponential decrease in particle displacements over the same range of packing fractions, implying the simultaneous existence of jammed and unjammed clusters in the evolving granular pack. This fragile state is characterized by developing contact stresses being spatially correlated with disk displacements. It is shown to arise as a consequence of nonzero friction which is known to introduce protocol

*Present address: Collective Interactions Unit, OIST Graduate University, 1919-1 Tancha, Onna-son, Kunigami-gun, Okinawa, Japan 904-0495; bandi@oist.jp

dependence on experimental measurements and is in accord with prior experimental observations [5,11]. These results are interpreted as a percolation of stressed contacts which exponentially decrease the fractional area enclosed within stress chains (defined by a threshold stress) over the range of packing fractions ($\phi_1 < \phi < \phi_2$). The fragile state and its associated stress percolation mechanism fall within a broader set of recent results that show existence of a fragile regime in the approach to jamming, including contact percolation [17], contact dynamics in granular glasses [13], and shear induced jamming that causes force network percolation [12].

We note the term *fragile* here denotes a mechanically metastable configuration—it is easily destroyed under the slightest external perturbation such as nonzero granular temperature, as we show later in the article. This state should not be confused with fragility in glass formers as defined by Angell [18] to distinguish between strong and fragile glasses which exhibit Arrhenius and Vogel-Fulcher behavior, respectively [19]. Although related to glasses within the broader context of disordered systems, this work does not concern itself with glass phenomenology in particular.

(iii) Under repetitive loading and unloading, we observe the critical packing fraction ϕ_c at which the granular pack jams progressively increases to higher values, thereby exhibiting creep. At the same time, the pressure curves for the loading-unloading cycles exhibit hysteretic responses. Relevant in the geophysical context [20,21], this hysteretic creep is experimentally shown to arise from interparticulate contact friction.

In Sec. II, we present a brief review of frictionless granular jamming and how friction changes the predictions expected to hold under idealized conditions. In Sec. III, we explain our experimental setup and the experimental protocol we follow in conducting our measurements. The main results of this study are presented in Sec. IV, followed by discussion and interpretation of these results in Sec. V, with a brief summary of results in Sec. VI.

II. BACKGROUND: GRANULAR JAMMING

A. Ideal jamming

The primary motivation for the jamming proposal [1] was to provide a common framework to describe the nonequilibrium behavior of a wide variety of disordered materials. O'Hern *et al.* [2] conducted extensive numerical studies with frictionless particles interacting via soft, finite-range, repulsive potentials at zero temperature and zero applied shear stress; henceforth, we refer to this set of specifications as *ideal granular jamming*. They reported many interesting properties of the ideal jamming transition around ϕ_c that have since been verified by mean-field theories [3,4] and experiments [5]. For a finite number of particles N, ϕ_c is a configuration-dependent random variable, the full width at half maximum of whose distribution was empirically determined [2] to follow the formula $w = w_0 N^{-\Omega}$ (where $w_0 = 0.16 \pm 0.04$ and $\Omega = 0.55 \pm 0.03$). O'Hern *et al.* found ϕ_c is sharply defined in the limit of infinite system size ($N \to \infty$), where ϕ_c coincides with random close packed density ($\phi_{\mathrm{RCP}} = 0.64$ in 3D and 0.84 in 2D), a concept first introduced by J. D. Bernal [22–24] to understand liquids which are structurally disordered by construction. We note, however, that difference of opinion exists within the community both with respect to the definition of random close packing [25] itself, as well as its coincidence with ϕ_c in granular jamming [26,27]. These divergent opinions notwithstanding, the existence of a ϕ_c where the jamming transition occurs is not in question.

The behavior of two quantities is of particular interest for the ideal jamming transition. The pressure P is zero below ϕ_c and rises continuously above ϕ_c as a power law [$P \propto (\phi - \phi_c)^{\psi}$ for $\phi > \phi_c$], whereas the coordination number $Z = 0$ below ϕ_c and undergoes a discontinuous jump to a critical value $Z = Z_c$ at $\phi = \phi_c$, followed by a power-law increase above ϕ_c, $(Z - Z_c) \propto (\phi - \phi_c)^{\beta}$. The critical coordination number $Z_c = 2D$ (D being the system's dimensionality) for frictionless particles, since ϕ_c is the system's isostatic point at which the total number of degrees of freedom equal the total number of constraints providing force balance.

The definition of a contact plays a central role here. A granular contact is said to exist when two particles come in physical contact and propagate a stress; albeit necessary, a stress-free physical contact is deemed insufficient. This requirement gives rise to a crucial and, perhaps, little-appreciated interpretation of the jamming transition. The discontinuous jump in Z from 0 to Z_c at ϕ_c implies that there are no contacts in the system up to ϕ_c—it may lose floppy modes and become rigid, but it is not stressed and, therefore, has zero granular contacts. At ϕ_c, a pressure rise above zero simultaneously activates contacts system wide due to stress propagation, and Z discontinuously jumps from 0 to Z_c. Because of the additional stress requirement in contact definition, granular jamming ideas make no allowance for a system to lie in an intermediate regime where part of the system is jammed and the rest is not—the only two states permitted are total systemwide jamming or lack thereof.

B. Frictional jamming

An increasing number of studies [6–9,11–13,16,28] have explored the role of friction and how it changes the ideal jamming predictions. Although a general framework for frictional packs has yet to emerge, studies indicate deviations from ideal jamming predictions. First, in addition to the normal component of force (F_N), friction gives rise to a tangential component (F_T). Second, the preparation method and history of the pack become important for frictional packs [28]. Treating the tangential force component as a new independent degree of freedom (at least for low friction coefficients) sets the critical coordination number at ϕ_c to lie in the range $D + 1 \leqslant Z_c \leqslant 2D$, i.e., hypostatic configurations are permissible. The condition $Z_c < 2D$ implies that frictional packs can jam at $\phi_c < \phi_{\mathrm{RCP}}$, with ϕ_c progressively decreasing with increasing μ before asymptoting to a constant value that has been termed random loose packing density ϕ_{RLP} [16]. ϕ_{RLP} is an empirically determined value from numerical simulations; its theoretical underpinnings are not well understood [10]. The same arguments made against the definition of ϕ_{RCP} [25] apply to ϕ_{RLP}.

Recent experiments in frictional systems also demonstrate a percolation mechanism in stress [12] en route to jamming

as well as in the steady-state contact dynamics [13] within the jammed regime. An experimental study by Cheng *et al.* [11] has also reported jamming of particles into a metastable configuration due to interparticle friction, which is readily destroyed under external perturbation or, alternatively, application of nonzero granular temperature.

III. EXPERIMENT

A. Description of the experimental setup

Figure 1(a) shows a schematic of the experimental setup. The system consists of a bidisperse mixture of 950 large (diameter $d_L = 0.9525 \pm 0.0025$ cm) and 950 small (diameter $d_S = 0.635 \pm 0.0025$ cm) disks of thickness 0.508 cm. The disks are placed in a chamber, with dimensions $L = 25.9$ cm and $W = 48.2$ cm (L is the compression direction), consisting of two glass plates held 0.635 cm apart by means of an acrylic frame that runs along the system's perimeter. Two movable boundaries are placed on the acrylic frame with aluminum plates that can slide back and forth within the chamber from opposite ends. The transverse boundaries are held fixed. The positions of the movable boundaries are controlled by two micrometers with a precision of 0.001 cm. Taking variations in radii into account for the given system of 1900 disks, this translates to a precision $\Delta\phi = 1 \times 10^{-5}$ in the packing fraction and, hence, serves as the lower bound on the quasistatic step size ($\Delta\phi$). All measurements reported in this article, however, were made at a quasistatic step size of $\Delta\phi = 1 \times 10^{-4}$, 3.5×10^{-4}, or 7×10^{-4}. The packing fraction (ϕ) is defined as the ratio of the area occupied by the disks to the total chamber area. The packing fraction is, therefore, controlled by changing the chamber area in this experiment. A set of six sensors [labeled A through F in Fig. 1(a)] placed along the boundaries measure the global two-dimensional pressure (N/m). Visual measurements using a Nikon D-90 camera (12.3 megapixel resolution) yield positions and displacements of individual disks.

Measurements were performed with disks machined from different materials spanning a range of experimentally determined static friction coefficients. The majority of the measurements were conducted with polymer disks that exhibit stress birefringence or photoelastic response (PE, static friction coefficient $\mu = 0.19$, elastic modulus $E = 2.5$ GPa). Measurements were also performed with photoelastic disks lubricated with graphite dust (PEG, $\mu = 0.14$, $E = 2.5$ GPa), photoelastic disks soaked in ethanol for 24 h which changed the modulus (PEA, $\mu = 0.19$, $E = 0.004$ GPa), lexan polycarbonate disks intentionally machined rough to obtain a high friction coefficient (LEX, $\mu = 0.22$, $E = 2$ GPa), and Teflon disks with an intrinsically low friction coefficient (TEF, $\mu = 0.06$, $E = 0.5$ GPa).

B. Measurement of static friction coefficient μ

A schematic of the apparatus used to measure the static friction coefficient is shown in Fig. 1(c). Four disks (of the same material) of diameter $d_L = 0.9525$ cm are arranged as shown in Fig. 1(c). The upper disk and the two bottom disks are held fixed and not allowed to rotate. A mass M is suspended

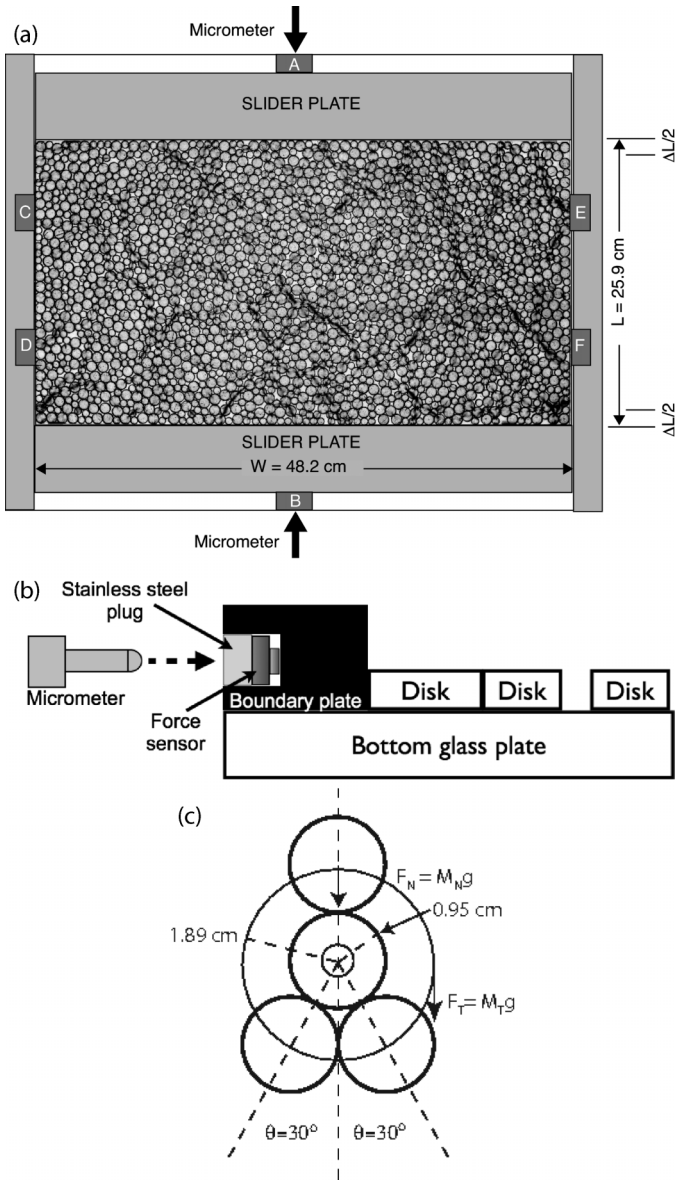

FIG. 1. (a) Experimental schematic: The system consists of 950 large and 950 small disks (ratio of radii 1:1.5). Two movable boundaries at opposite ends control the system's packing fraction ϕ and are used to provide uniaxial, quasistatic compression. Force sensors labeled A through F in the schematic measure the boundary pressure. The image is contrast enhanced data for $\phi = 0.8113$. (b) Side view schematic of force sensor placement within the compression boundary. When the micrometer (left) pushes on the boundary plate to its right, the force sensor registers the cumulative force of the boundary plate and granular pack. (c) Schematic of the static friction coefficient measurement apparatus. Four disks of diameter $d_L = 0.9525$ cm are placed in contact with each other as shown in the schematic. The three outer disks are held fixed and have no translational or rotational degrees of freedom. The middle disk can be rotated by means of an external lever. A normal force $F_N = M_N g$ is applied by a suspended weight of mass M_N on the top disk. This force is transferred to the disk sandwiched in the middle, which in turn transfers it to the two bottom disks at an angle of 30°. A tangential force $F_T = M_T g$ applied on the middle disk allows it to slip at a critical force, which allows determination of the static friction coefficient μ for the disks.

TABLE I. Experimentally determined values of μ for indicated materials (abbreviations defined in text) and their elastic modulii E (supplied by manufacturer).

Material	Friction Coefficient μ	Modulus E (GPa)
PE	0.19	2.5
PEG	0.14	2.5
PEA	0.19	0.004
LEX	0.22	2.0
TEF	0.06	0.5

from the upper disk such that a force $F_a = Mg$ is applied vertically down by the upper disk onto the central disk. A tangential force $F_m = mg$ is applied on the central disk (free to rotate) via a pulley system where a mass m is attached to the pulley with diameter $d_p = 1.887$ cm. Mass is added to m until slip events occur. In practice, the weights are placed in a receptacle of mass 29 g, hence $F_m = (m + 29)$g. Due to the torque ratio, the actual tangential force applied on the central disk is $F_T = F_m d_p/d$. The normal force on the central disk arises from the three (one top and two bottom) disks in contact with it. The vertical disks apply a normal force $F_{Nu} = F_a$, whereas the bottom disks must balance this vertical force. Hence, F_a is equally divided between the two bottom disks giving $F_a = 2F_{Nb}\cos\theta$. The total normal force is $F_{Nu} + 2F_{Nb} = F_a + F_a/\cos\theta = F_a(1 + 1/\cos\theta)$.

The ratio of the total normal force applied to the total tangential force required for a slip to occur in the central disk provides a measure of the static friction coefficient μ. Plugging in values for $d_P/d_L = 1.98$ and $(1 + 1/\cos\theta) = 2.15$ with $\theta = 30^\circ$, we get

$$\mu = \frac{F_T}{F_N} = \frac{F_m d_P/d}{F_a(1 + 1/\cos\theta)} = \frac{1.98F_m}{2.15F_a} = 0.92\frac{F_m}{F_a}. \quad (1)$$

Values of the static friction coefficients for each of the materials used in this study are listed in Table I.

C. Experimental protocol

We initially place all disks in the interrogation chamber in random positions and move the boundary plates to an initial packing fraction chosen *a priori* to fall comfortably in an unjammed state. The disks are subject to friction (with the glass bottom, the boundary and with each other) and the system jams below the random close packed density $\phi_{\mathrm{RCP}} \approx 0.84$. After each quasistatic step, a 10-s time-trace of all six boundary sensors is collected at a sampling frequency of 1 KHz followed by a digital image of the whole system. The time-averaged value of the trace constitutes the pressure measured by the boundary sensor at a particular value of ϕ. The boundaries are then moved through a quasistatic step ($\Delta\phi$), and the procedure is repeated. The only control parameter in this experiment is the quasistatic step $\Delta\phi$. No other external excitation or perturbation is applied. As a consequence, this experiment studies the pack evolution at "zero granular temperature." Unlike ideal jamming, real-world experiments have to contend with friction. Usually, frictional effects are circumvented by applying a granular temperature via acoustic excitation or vibration of boundaries that relax frictional stresses. In the absence of any such mechanism in this experiment, frictional effects become fully manifest. The ideal jamming requirements of zero temperature and zero friction are, experimentally, mutually incompatible. Meeting the zero friction requirement violates the zero temperature requirement and vice versa. Second, we do not tap the system after each quasistatic step to mimic annealing in simulations [5]. Tapping the system in experiments (or annealing in simulations via gradient minimization or alternative methods), no matter for how short a duration or how weak in amplitude, is tantamount to application of an effective granular temperature which violates the zero temperature requirement. In order to understand the role of granular temperature, we performed one experimental run, discussed below, where the system is subjected to gentle (but systematically uncontrolled) tapping after each quasistatic step.

D. Experimental systematics

The noise floor (instrumental noise) of the boundary pressure sensors is about 0.1 N/m. Accordingly, sensors C-F [see Fig. 1(a)] placed along the immovable transverse direction register 0.0 ± 0.1 N/m pressure when the system is unjammed. On the other hand, sensors A and B [see Fig. 1(a)] placed along the movable, compression direction register an offset of about 11 N/m. As shown in Fig. 1(b), the compression axis sensors were placed within the movable boundary plate. As per the experimental protocol, the initial boundaries were set to a predetermined packing fraction that lies well below the jamming threshold. At this point the micrometers were detached from the boundary, and a baseline pressure trace was recorded to measure the instrumental noise. This was considered prudent, despite the sensors being driven by homebuilt voltage regulator circuits designed for stability against thermal drift. Furthermore, the 10-s pressure time-trace recorded at 1 KHz averages the instrumental noise. Like the transverse axis sensors (C–F), the compression axis sensors (A and B) also register 0.0 ± 0.1 N/m pressure reading when the micrometers are detached from the boundary plates. When, however, a micrometer comes in contact with the boundary plate and pushes against it, a pressure offset of 11 N/m is registered. This pressure jump for compression axis pressure can be seen in the inset of Fig. 4(a). When the micrometers are advanced through a quasistatic step $\Delta\phi$, they directly push against a stainless steel plug that protects the sensor housed in a groove within the boundary plate. The sensor in turn pushes against the boundary plate. As a consequence, the boundary plate's friction with the bottom glass plate gives rise to the 11-N/m offset.

In the data presented in the following [in particular, please see the inset of Fig. 4(a)], a 11-N/m offset was added to the pressure signals for immovable transverse axis sensors to render them co-incident with the compression axis pressure scaling. Offset addition to transverse axis pressure was preferred over offset subtraction of compression axis signals for a practical reason. Offset subtraction of compression signal causes some fluctuations to go negative, causing chopping of negative fluctuations when the data is plotted on a log-linear scale [Fig. 4(b)].

In order to ascertain the magnitude of this systematic error in measured compression pressure, we modified the arrangement of pressure sensors. In particular, rather than measure the pressure at a position between the compression micrometer and the movable boundary, two sensors (as opposed to one) at the two ends of the movable plate were placed near a very small and light frame located near the disks. This did reduce the offset to 0.25 ± 0.01 N/m, but the need for a small and light frame also means it bends at the center due to the slight, unavoidable bulge of the sensors required so they alone make contact with the frame. This creates a different systematic error in the experiment. The results obtained were very similar in this case, but we place more confidence in the more extensive measurements made with the first design.

As the compression boundary moves in and mobilizes an increasing fraction of disks, the friction between disks and the bottom glass plate is registered through a linear ramp of small, but measurable, slope in pressure. A portion of this ramp is discernible in the prejamming threshold data presented in Fig. 4(b). The presence of a top glass confining plate was also considered. The number and variety of runs with this modified apparatus were small compared to those taken with the primary apparatus whose results we discuss here. The general characteristics of the results are the same for both experiments.

Although photoelastic disks were employed to discern the spatial stress distribution, the photoelastic threshold was rather high due to high stiffness of the material used. As a result, photoelastic stress signals were not visible well into the rise in the system's global pressure measured with boundary sensors. Due to this design property, we were unable to provide measurements of the coordination number Z in this study.

IV. RESULTS

A. First loading cycle: Jamming onset in presence of friction

Here we discuss the role of friction on the onset of jamming when the pack is compressed the first time from a random initial configuration. Silbert *et al.* have shown [7,16] that the critical coordination number Z_c as well as the critical packing fraction ϕ_c at which jamming occurs shift to progressively lower values with increasing friction coefficient, due to the additional structural stability provided by the tangential forces. Analysis for jamming [7] and for the unjamming transition [16] reached similar conclusions. In Fig. 2 we plot the pressure P versus packing fraction ϕ for disks with different friction coefficients (Z is not measured for reasons discussed in Sec. III D). Treating commencement of pressure rise as the jamming onset condition, we confirm the numerical prediction of Silbert *et al.* that jamming onset does occur at lower packing fractions with increasing friction. Whereas jamming onset also represents the jamming transition in *ideal jamming*, the same is not true in this experiment. Here the term *jamming onset* marks the nucleation of the first jammed cluster within the system. Unlike *ideal jamming*, which is marked by an abrupt transition, in this experiment the jamming transition proceeds smoothly through a stress percolation mechanism, as we discuss in Sec. IV B.

The range of friction coefficients $0.06 \leqslant \mu \leqslant 0.22$ for disks employed in this study yields friction-dependent values

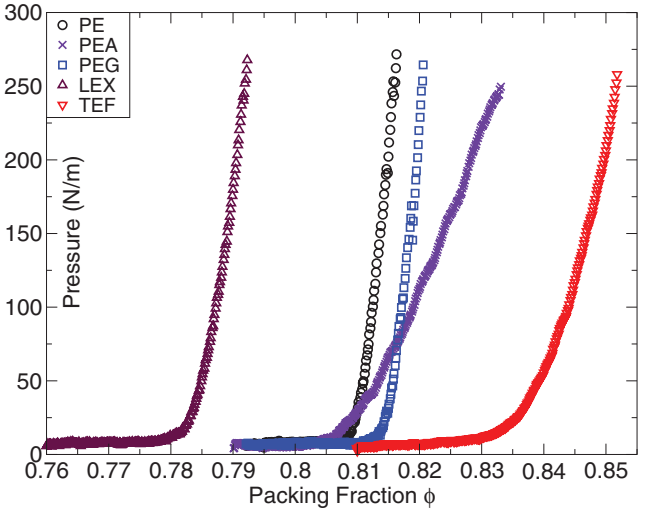

FIG. 2. (Color online) P vs ϕ (quasistatic step size $\Delta\phi = 1 \times 10^{-4}$). The packing fraction ϕ at which system pressure starts increasing monotonically falls with increasing static friction coefficient μ. The change in pressure slopes arises from different elastic moduli of the materials used.

of the critical packing fraction ϕ_c that are greater than the asymptotic steady value corresponding to random loose packing (ϕ_{RLP}); one would need higher μ to reach RLP conditions. Nevertheless, the experimental values of ϕ_c we measure for the experimental values of μ are close to those obtained in numerical simulations of Silbert *et al.* (see Fig. 1 and Table 1 of Ref. [16]). Since we use different materials with varying elastic moduli, the slopes of the pressure curves vary between the materials. As a counterpoint, a quick comparison of PE and PEG data shows that the two plots have the same slope since they have the same modulus. Since PEA disks are softer, however, they have a shallower slope in comparison to PE data, but the pressure rise does approximately coincide for both PE and PEA data since they share the same friction coefficient. The slight difference in the ϕ value of pressure rise start between PE and PEA can be attributed to configuration-dependent fluctuations that naturally arise among different experimental runs.

In Fig. 3, we show the variation of the critical packing fraction ϕ_c as a function of the disk friction coefficient μ. In particular, the quantity $1 - \phi_c/\phi_{\mathrm{RCP}}$, the fractional deviation from the expected zero friction random close packed value ϕ_{RCP}, increases consistently with a linear dependence on μ, again agreeing with numerical simulations [16].

B. First loading cycle: Fragile behavior

We next consider the shape of the pressure curve itself by comparing the pressure signal for the first and second jamming cycles. Figure 4(a) plots P from one compression boundary sensor versus ϕ for the first and second jamming cycles for photoelastic disks (PE). The continuous increase in P for the first cycle differs qualitatively from the more abrupt change in slope for the second cycle. The lateral shift in P is a signature of a friction-induced hysteretic response which progressively shifts ϕ_c to higher values as the system is repeatedly jammed and unjammed (discussed below in Sec. IV C). The vertical

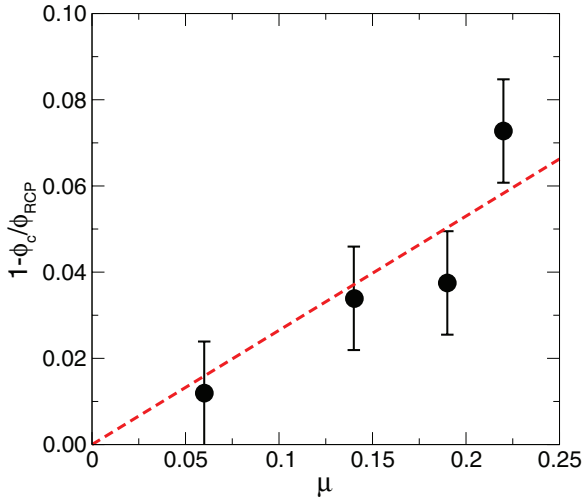

FIG. 3. (Color online) Deviation of fractional ϕ_c with respect to ϕ_{RCP} vs μ for materials described in Fig. 2. The error bars are estimates as opposed to statistical averages over many runs.

shift in P within the flat (unjammed) regime for the first cycle [black circles in Fig. 4(a)] is traced to the friction between the movable boundary plates plus the mobilized fraction of disks and the glass bottom as explained in Sec. III B. At the end of the first loading cycle, when the system is decompressed, the boundary plates only move back until stresses in the pack are relieved. Further quasistatic reverse stepping of micrometers does not cause continued backward motion of boundary plates to their initial positions. Instead, the micrometers decouple (loss of physical contact) from the boundary plates. For this reason, the unjammed regime observed during the second compression cycle [red squares in Fig. 4(a)] does not show the vertical shift in P. During the first cycle, the boundaries move in and push the disks towards a jammed configuration. When unjammed and jammed again, the contacts that were developed at the end of the first jamming cycle are reactivated, and the stresses build up as the system is subjected again to uniaxial compression.

To better understand the smooth increase in P for the first jamming cycle, Fig. 4(b) plots P versus ϕ on a log-linear scale. One sees three distinct regimes in the pressure curve. In the unjammed (consolidation regime) P is essentially flat, modulo a shallow ramp due to friction between disks and bottom glass plate. The second regime is characterized by an exponential increase in P beginning at $\phi_1 \approx 0.8093$. The solid line in Fig. 4(b) is an exponential fit to the data $P \propto e^{\phi/\chi_P}$ with $\chi_P = 0.00195$. Note that although the range of ϕ for the exponential regime is small, the increase in P over that interval is almost one decade. The pressure eventually deviates from this exponential regime and settles to a regime that seems to fit well with linear scaling [dashed line in Fig. 4(b)] $P \propto (\phi - \phi_2)$. Due to a limited range of pressure data for $\phi > \phi_2$, it is not clear whether this regime scales linearly or algebraically ($P \propto \phi^{\psi}$) with the exponent ψ being marginally greater than 1. The inset in Fig. 4(a) plots P from all four boundaries against ϕ on a linear scale. The remarkably good collapse of the pressure curves atop one another strongly suggests that anisotropic effects arising from uniaxial compression are not detected

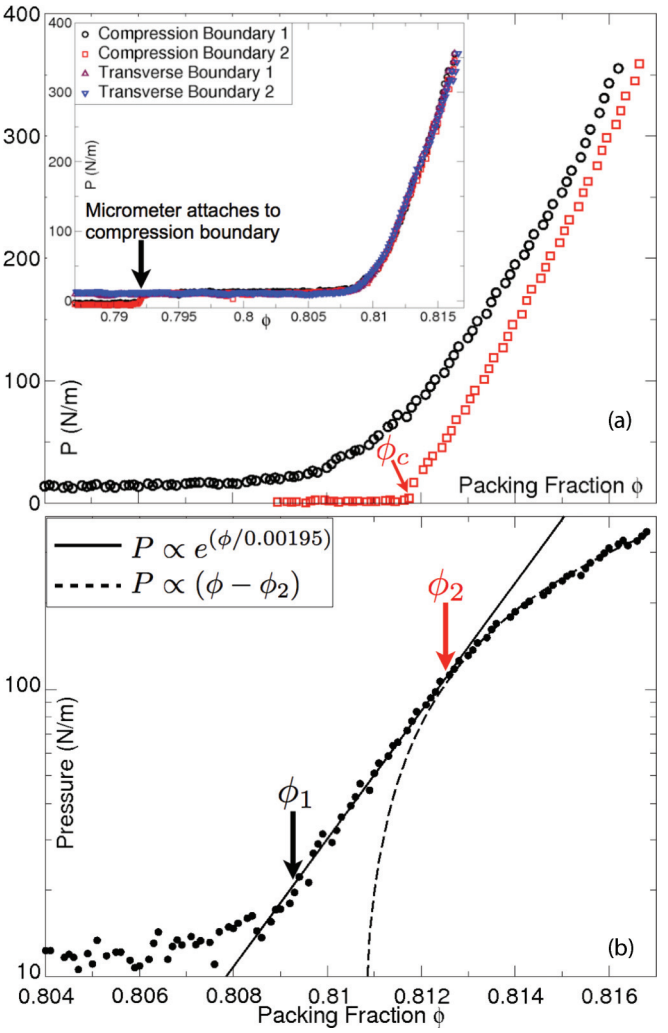

FIG. 4. (Color online) (a) P vs ϕ (linear scale) for the first (black circles) and second (red squares) compression cycles. The pressure scaling is gradual for the first cycle as compared to the more abrupt transition during the second cycle where ϕ_c is indicated. The inset plots the pressure from all four boundaries (same vertical and horizontal scale). No anisotropy is observed in the pressure signal. (b) P vs ϕ for the first jamming cycle (log-linear scale) shows the existence of an intermediate regime where pressure scales exponentially. The solid line is an exponential fit to the data $P \propto e^{\phi/\chi_P}$ with $\chi_P = 0.00195$, and the dashed line is a linear fit. The values of ϕ_1 and ϕ_2 are indicated in the plot.

by the pressure sensors. This isotropy may result from our geometry for which the aspect ratio is $L/W = 0.54$ and would probably not persist for large aspect ratios, i.e., $L/W \gg 1$.

Although this exponential pressure scaling for the first loading cycle seems to contradict the predicted [2,3,5] power law for P across the jamming transition, as we will discuss below, it can be explained through a stress percolation mechanism. The predicted power-law scaling (approximately linear[1]) is, however, recovered for subsequent jamming cycles

[1]The best fit of the data to the form $P \propto (\phi - \phi_c)^{\beta}$ yields $\beta = 1.1$, consistent with Ref. [5].

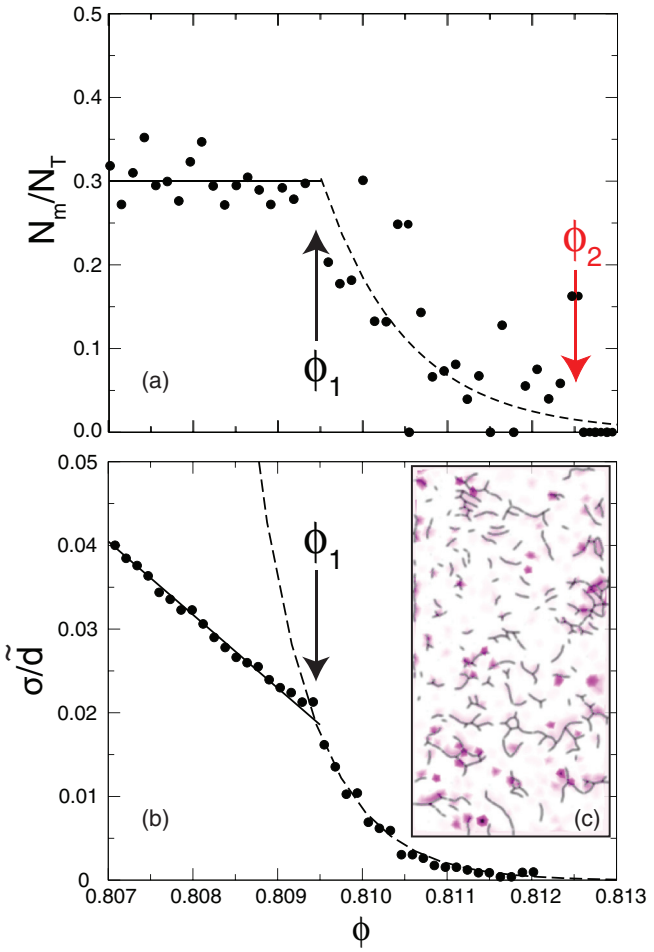

FIG. 5. (Color online) (a) Fraction of disks moving N_m/N_T vs ϕ showing a constant region for $\phi < \phi_1$ and exponential decay for the fragile regime ($\phi_1 < \phi < \phi_2$) with $\chi_N \approx 0.001$. (b) Normalized displacement variance $\sigma/\tilde{d}$ relative to a state near ϕ_2 showing a linear decrease for $\phi < \phi_1$ and an exponential decrease with $\chi_\sigma = 0.0007$ for the fragile regime ($\phi_1 < \phi < \phi_2$). (c) Image of the superposition of the difference in the stress network (black lines) and the magnitude of disk displacements between $\phi = 0.8095$ and $\phi = 0.8105$. Arrows indicate ϕ_1 and ϕ_2.

as shown for the second jamming cycle in Fig. 4(a), where $\phi_c = 0.8118$ is determined by the point at which P starts to rise.

We now look at the behavior of disk displacements. Figure 5(a) shows the fraction of disks moving a distance greater than about 1% of a mean disk diameter[2] as a function of ϕ where N_m is the number moving and $N_T = 1900$ is the total number of disks. The fraction is constant at about 0.3 up to $\phi_1 = 0.8094$, after which it decreases rapidly up to the jamming value $\phi_2 = 0.8124$. The decrease is consistent with an exponential $e^{-\phi/\chi_N}$ with $\chi_N \approx 0.001$. The variance of individual disk displacements σ [normalized by $\tilde{d} = (d_L + d_S)/2 = 0.794$ cm] relative to a state near the jamming threshold[3] is shown in Fig. 5(b) as a function of ϕ. One again observes two distinct regimes: a linear one that corresponds to the unjammed (consolidation) regime where the pressure curve in Fig. 4(b) is flat and a second one in which the variance decreases exponentially with $\sigma \propto e^{-\phi/\chi_\sigma}$ with $\chi_\sigma = 0.0007$. This exponential drop in displacement variance occurs over the same interval in ϕ as the exponential regime of the pressure curve in Fig. 4(b) as indicated by the arrows depicting ϕ_1 and ϕ_2. The presence of disk displacements in the exponential regime, where a percolating force network already exists, suggests that the particles that are part of the force network still undergo small displacements and deformations, which in turn allows visible displacement *inside* the network region, eventually leading to the refining of the network.

The above picture is reinforced by the data in the inset Fig. 5(c), where the difference in the force chain network between $\phi = 0.8095$ and $\phi = 0.8105$ is shown as black lines and the spatial distribution of the magnitude of particle displacements is shown. The correlation of new stress chain creation (the differences) and the particle displacements, albeit striking, is not quantitative. Qualitatively, the formation of a new stress chain is not spatially correlated with disk displacement magnitudes but rather with the presence or absence of displacements. We followed the simple procedure described below to quantify this spatial correlation. For each new stress contact formed between two disks during a quasistatic step, we considered the center of the line joining the two disk centers. An annulus of inner radius r and outer radius $(r + \Delta r)$ was considered [$\Delta r = \tilde{d} = (d_L + d_S)/2$, the average diameter of one small and one large disk]. Please see the schematic inset in Fig. 6. The ratio of the number of displaced disk centers N_d to the total number of disk centers counted within the annulus N_c was measured for increasing distances of r in multiples of $\tilde{d}$. The procedure was repeated for each new stress chain formed during a quasistatic step at several radial distances r and averaged over.

Figure 6 plots the average ratio $\langle N_d/N_c \rangle$ versus the dimensionless radial distance $(r + \Delta r)/\tilde{d}$. The bar graph represents the value within the annular region of width Δr for increasing inner radial distance r (in multiples of $\tilde{d}$). The integrated value of this quantity is plotted in (red) solid circles representing the cumulative fraction $\langle N_d/N_c \rangle$ for the circle of radius $(r + \Delta r)$. The value at $r/\tilde{d} = 1$ is biased because it can only include small disk centers ($d < \tilde{d}$) within that radial distance. A little over 40% of the disks are mobilized within $(r + \Delta r) = 3\tilde{d}$ from the center of the newly formed stress chain. $\langle N_d/N_c \rangle$ abruptly falls for $(r + \Delta r) > 3\tilde{d}$, implying a majority of disk displacements occur within the vicinity of a newly formed stress chain. This boundary is denoted by a vertical dotted line in Fig. 6; this dotted vertical line is merely a visual indicator. The ratio $\langle N_d/N_c \rangle \neq 0$ for $(r + \Delta r) > 3\tilde{d}$ for two reasons. First, there are displacements in unjammed regions of the granular pack where no new stress chains form. Second, these displacements do contribute indirectly to

[2]There are smaller displacements below our threshold that may behave differently as a function of ϕ.

[3]Picking different reference states near or beyond jamming causes a finite offset in variance of different magnitudes, but the exponential decay is preserved with the same value of $\chi = 0.0007$ to within experimental precision.

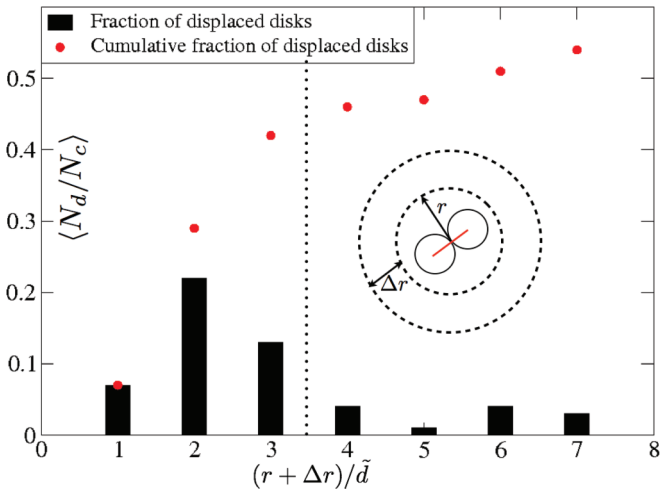

FIG. 6. (Color online) Bar graph shows the number of displaced disk centers N_d normalized by total number of disks N_c counted within an annulus of width Δr at a radial distance r from the center of a newly formed stress chain (see schematic in the inset) vs the dimensionless radial distance $(r + \Delta r)/\tilde{d}$ from the center of a newly formed stress chain [$\tilde{d} = (d_L + d_S)/2$ is the average diameter of the large and small disk]. The solid circles (red) present the cumulative fraction $\langle N_d/N_c \rangle$ within the radius $r + \Delta r$. The vertical dotted line is a marker indicating the radial distance beyond which an abrupt fall in $\langle N_d/N_c \rangle$ is observed.

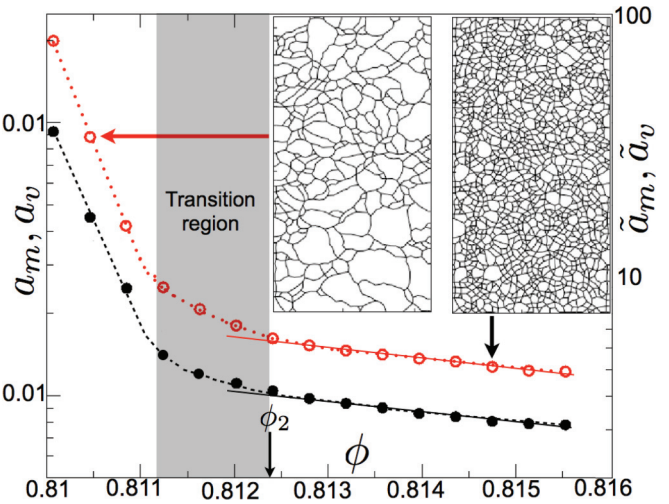

FIG. 7. (Color online) Log-linear plot of the mean (•, black solid circles in lower curve) and variance (○, red circles in upper curve) of stress chain domain area normalized by total area, a_m, a_v (left axis) or by the mean area formed by connections between different combinations of three disks in a close packed triangular array, $\tilde{a}_m$, $\tilde{a}_v$ (right axis), respectively. Insets show stress networks and corresponding domains for $\phi = 0.8104$ (left) and $\phi = 0.8148$ (right). The dashed (lower curve) and dotted (upper curve) lines are fits to a combined linear dependence with a decaying exponential (see main text) for a_m and a_v, respectively. The grayscale region highlights the transition from exponential to linear behavior under compression. The solid red and black lines are markers included to indicate the end of transition from exponential to linear behavior near $\phi_2 = 0.8124$.

new stress chain formation at distances $(r + \Delta r) > 3\tilde{d}$ in the sense that they communicate displacements from the moving boundary to the location where the stress chain forms.

To further study the nature of the different regimes observed in global pressure measurements, we consider local properties of disk configurations, namely the structure of stress chains. The identified stress chains enclose domains with no measured stress as illustrated in the insets of Fig. 7. We characterize the stress chain networks by the mean a_m and variance a_v of the fractional domain area (relative to the total cell area on the left axis) and also by the mean $\tilde{a}_m$ and variance $\tilde{a}_v$ of the domain area but now normalized (right axis) by the average of the area enclosed by a triangular arrangement of small and large disks (all large, all small, two large, two small). As indicated in the inset images, the mean and variance decrease rapidly between 0.810 (the lowest value of ϕ for which we could determine the stress chain network) and $\phi_2 = 0.8124$. For higher $\phi >$ 0.8124, the mean and variance decrease linearly with a small slope. Fits to an exponentially decreasing function $e^{-\phi/\chi_s}$ as shown in Fig. 5 yields the same value of $\chi_s = 0.00035$. The exponential decrease in a_m and a_v is another signature of the fragile jammed state. The transition from exponential to linear behavior occurs over a short range of packing fractions highlighted in grayscale in Fig. 7. The end of this transition regime coincides with $\phi_2 = 0.8124$. Solid line fits of the linear regime are included to highlight the deviation from transition regime to linear behavior at ϕ_2 (please see Fig. 7).

As a control, we also conducted one experimental run where the system was subjected to gentle (but systematically uncontrolled) tapping after each quasistatic step during the first compression cycle for multiple reasons. First, we wanted to verify that our granular system reproduced the results of Majmudar *et al.* [5] since the essential point of departure between the two measurements lies in the protocol—namely tapping the system to mimic annealing. Accordingly, we recovered their result for the jamming transition (see Fig. 8) although the corresponding ϕ_c is still below $\phi_{\mathrm{RCP}} = 0.84$. We attribute the discrepancy to two possibilities. First, we do not

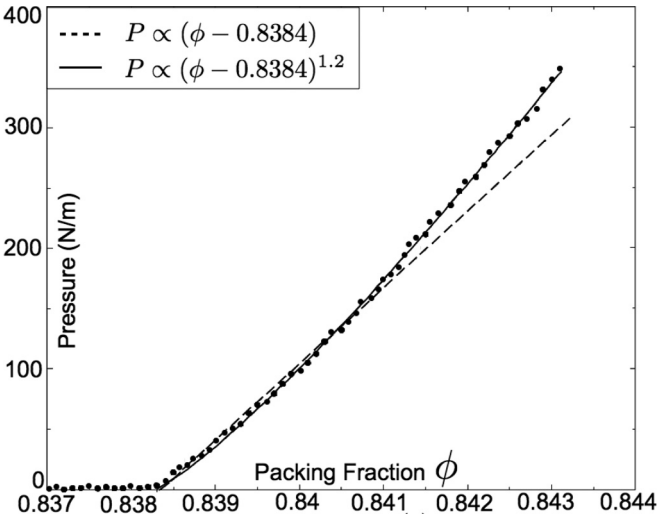

FIG. 8. P vs ϕ for first compression cycle where the system is gently tapped (albeit with no systematic control) after each quasistatic step.

systematically control the tapping process. We merely tapped the system along the four boundaries gently with a mallet after each quasistatic cycle. Hence, the plot in Fig. 8 only serves as qualitative verification. Second, the discrepancy can be attributed to our system size, $N = 1900$ disks. Based on the numerical studies of O'Hern *et al.* [2], where ϕ_c was shown to be a configuration dependent random variable for finite system size, it is possible that the control experiment we performed had a configuration that jammed marginally below ϕ_{RCP}. Finally, as noted in Sec. II A, the location of ϕ_c relative to ϕ_{RCP} not withstanding, the scaling properties about ϕ_c are robust.

The control run for the first loading cycle with tapping is an excellent example of how the presence of friction makes pack evolution strongly protocol dependent: In the absence of external perturbations the pack exhibits exponential scaling, but with tapping it exhibits power-law scaling. In addition, this control run also points to another subtle feature of the jamming paradigm. The ideal jamming predictions are predicated on the requirements of zero friction, zero temperature, and zero applied stress. The results observed with and without tapping show us zero friction and zero temperature are incompatible requirements in the real world where one cannot escape frictional effects, save in strong exceptions like jamming in foam. One then begs to ask, if tapping [5] is considered equivalent to annealing processes invoked in simulations, is the zero temperature requirement being adhered to? Also, if one interprets tapping as a thermal kick (rather than a constant thermal agitation), it is tantamount to destroying the system's evolution history after each quasistatic step. Then are the ideal jamming predictions a result of a protocol that renders the pack memoryless? Whereas the hysteresis results (a memory effect) to follow in Sec. IV C, suggest tapping destroys pack memory in our system, we note that tapping could presumably also destroy a developing heterogeneous configuration where the granular solid and liquid phases coexist. It is not clear from our experiments whether tapping destroys memory, homogenizes an evolving heterogeneous configuration, or both. We believe these are important issues that merit further work, since thermalization can act both to render a system memoryless as in the present instance or help to retain system memory [29].

Finally, we present a result that bridges the fragile behavior just discussed with the third primary result of this study, namely friction-induced hysteresis and creep. In Fig. 9, we plot the pressure from the compression boundary sensor against packing fraction for photoelastic (PE) disks ($\mu = 0.19$ and $E = 2.5$ GPa) for three different quasistatic step sizes, $\Delta\phi = 1 \times 10^{-4}$, 3.5×10^{-4}, and 7×10^{-4}. The data belong to the first compression cycle as evidenced by the smooth pressure increase expected for the fragile regime. Figures 4, 9, and 10 present data from different experimental runs of the first compression cycle to underscore the robustness of fragile behavior we have argued for in this subsection.

The same experimental protocol, as detailed in Sec. III C was followed to obtain the result plotted in Fig. 9. In particular, we emphasize that no tapping was employed (as done in the control run described immediately above) after each quasistatic step. All three curves follow the same slope for the exponential $\chi_P \sim 0.00195$. These experimental runs were repeated with varying wait times between quasistatic steps to explore the possibility of interstep annealing; no measurable

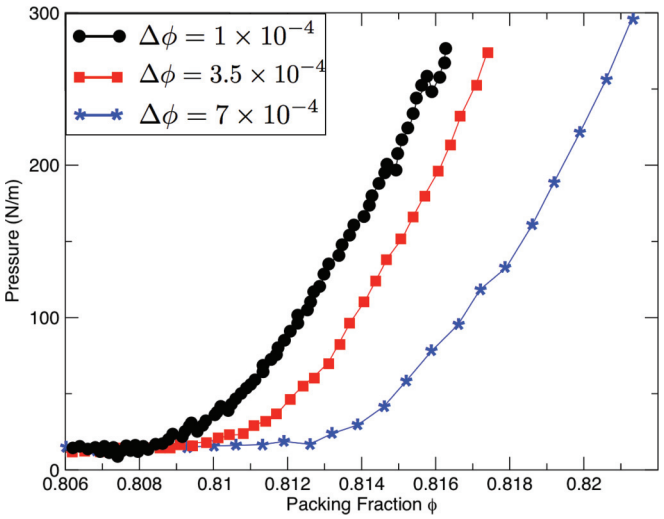

FIG. 9. (Color online) Pressure P from the compression sensor for the first compression cycle versus ϕ for PE disks ($\mu = 0.19$) jams at higher packing fractions with increasing step magnitude of quasistatic compression $\Delta\phi = 1 \times 10^{-4}$, 3.5×10^{-4}, and 7×10^{-4}.

change in signal was observed. Due to the strongly athermal nature of the system in question, the system state can only be changed through one of two mechanisms: perturbations that introduce a granular temperature such as the brief thermal kick provided by tapping or the quasistatic step $\Delta\phi$. The result in Fig. 9 falls in the latter category.

The pressure curves in Fig. 9 exhibit a monotonic increase in the jamming onset as the corresponding control parameter $\Delta\phi$ is increased, thereby suggesting the absence of a unique packing fraction at which a frictional pack jams into an irregular solid. As noted in Secs, II A and II B, the notion of a uniquely defined critical packing fraction for jamming onset (namely random close packing ϕ_{RCP} and random loose packing ϕ_{RLP}, respectively) is not universally accepted. Evidence to this effect comes from several studies for both frictionless [26] and frictional [28] systems that demonstrate a continuous range of

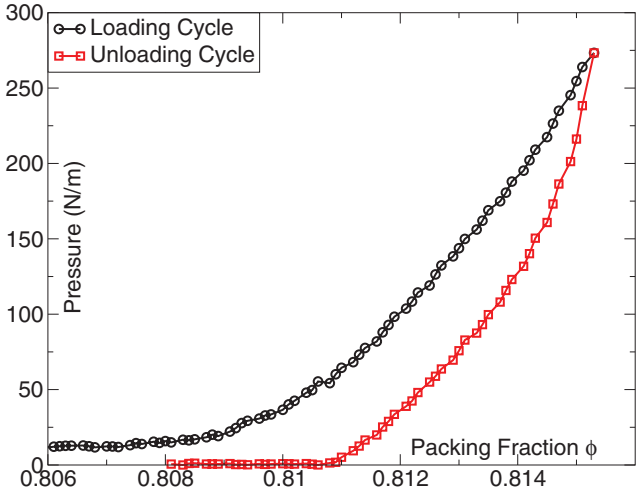

FIG. 10. (Color online) P vs ϕ (equivalent to stress-strain measurement) for PE disks at $\Delta\phi = 1 \times 10^{-4}$ exhibits hysteresis.

packing fractions over which jamming occurs. Therefore, the result we present in Fig. 9 is neither new, nor surprising in itself; yet a crucial distinction exists, as we explain in the following.

Of several sources that induce fluctuations in a granular system, including experimental and thermal noise protocols, configurations, annealing protocols, particle geometry and polydispersity, and friction coefficient, the sources relevant to this study are the experimental protocol, configuration dependent fluctuations, and friction coefficient. Unlike simulations, it is difficult for an experiment to cycle through a large set of configurations to seek out the average threshold packing fraction for jamming onset. For the five independent experimental runs presented in Fig. 9, all runs exhibited the monotonic dependence on $\Delta\phi$. The configuration-dependent fluctuations in jamming onset for a given run at a specified $\Delta\phi$ were never large enough to encroach on the jamming onset for a different $\Delta\phi$. Whereas we are unable to entirely discount the possibility that this effect arises from configurational fluctuations, our tests suggest this may not be the case. This effect is clearly protocol dependent. In addition to the tapping mechanism which changes the nature of the fragile regime, the dependence of jamming threshold on $\Delta\phi$ suggests a new type of protocol dependence.

In the thermal counterpart of jamming in liquids, namely the glass transition, the dependence on cooling rate of the approach to the transition is well known [30,31]. Further, in simulations of frictional jamming, Inagaki *et al.* [28] established the dependence of jamming onset ϕ_c on the annealing rate. All granular and glass studies, however, show that the approach to respective ϕ_c or T_g is delayed as the cooling rate is slowed. This is in contrast with our observation that increasing $\Delta\phi$ leads to jamming onset at higher packing fractions. In analogy with the cooling rate in liquids, if an analogous quasistatic rate $\frac{\Delta\phi}{m}$ (m is the number of quasistatic steps) were considered, it remains constant across all three runs in Fig. 9; doubling $\Delta\phi$ halves the number of experimental points, keeping their ratio constant. Further, we do not apply the experimental equivalent of an annealing protocol (interstep tapping) in these experiments. As we explain in the following subsection on friction-induced hysteretic creep, this result finds its origin in friction. This result does merit the question whether $\phi_1 \rightarrow$ constant (modulo fluctuations from other sources) as $\Delta\phi \rightarrow 0$. This question is beyond our experimental purview and is best explored through numerical simulations which offer access to infinitesimal step sizes.

C. Repetitive loading: Friction-induced hysteresis and creep

Following the first loading cycle, we now turn our attention to the role of friction under repetitive loading and unloading. Here we report two frictional effects that strongly deviate from current jamming predictions. When the granular pack is subjected to loading and unloading, hysteresis is observed in the pressure versus packing fraction plot (see Fig. 10). If subjected to repetitive loading-unloading cycles, the system exhibits creep, whereby the packing fraction at which the system jams progressively shifts and the hysteresis curves evolve towards higher packing fractions. Friction-induced hysteresis [32], as well as the rate-dependent behavior of ϕ_c

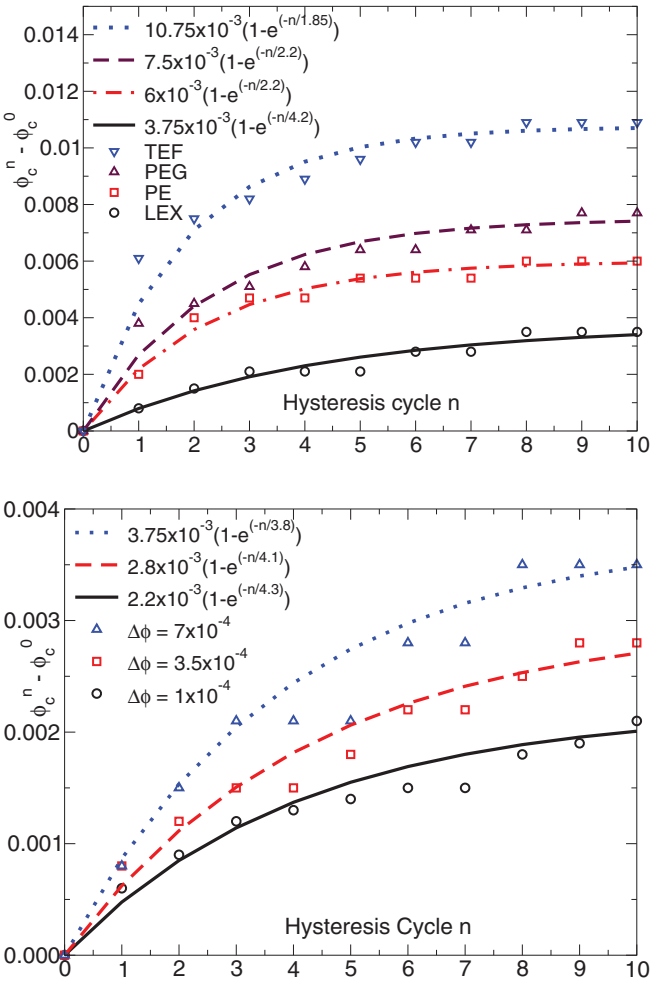

FIG. 11. (Color online) Top: Difference between ϕ_c^n and its initial onset value ϕ_c^0 as a function of the number of cycles of loading and unloading n for different materials. Bottom: Same quantities for the PE material and for different step sizes $\Delta\phi$. Materials and step sizes are labeled in the plot legends as are the coefficients in the solid-line exponential fits.

[28], have been reported recently. Because frictional jamming is heavily dependent on preparation protocol, we are unable to offer a comparison between our study and prior works. Nevertheless, since our experimental setup design shares close correspondence with standard mechanical load cell designs, it allows us to compare our results with relevant amorphous solids in the geophysical context (e.g., certain forms of sandstones and sedimentary rocks).

In Fig. 11 we plot the difference in ϕ_c between the n^{th} (ϕ_c^n) and 0^{th} (ϕ_c^0) loading-unloading cycles against the cycle number n. In the top panel we vary the friction coefficient μ while keeping the quasistatic step-size constant at $\Delta\phi = 1 \times 10^{-4}$, whereas in the bottom panel we keep the friction coefficient constant at $\mu = 0.19$ for PE disks, while varying the quasistatic step size $\Delta\phi$. The rate at which the pack evolves from ϕ_c to ϕ_{RCP} exhibits monotonic dependence on the friction coefficient with the pack evolution being quickest for TEF with lowest friction coefficient, followed by PEG, PE, and, finally, LEX with the highest friction coefficient. Also, as shown in the bottom panel in Fig. 11, the quasistatic step-size

$\Delta\phi$, which controls the magnitude of perturbation provided to the pack also controls the pack evolution rate monotonically at step sizes $\Delta\phi = 1 \times 10^{-4}$, 3.5×10^{-4}, and 7×10^{-4}, thereby exhibiting rate dependence in the pack evolution in a quasistatic sense. This rate dependence in hysteretic creep does not imply a reduction in width of the hysteresis loop with increasing cycle n. The hysteresis curves for all cycles, and for all quasistatic step sizes $\Delta\phi$, exhibit the same area within their loops for a given friction coefficient—this area within the hysteresis loop is the energy dissipated due to friction. Instead, this rate dependence implies, the lateral shift in the hysteresis loop decreases with increasing hysteresis cycle number n. Furthermore, once the granular pack eventually stabilizes and no further creep is measurable, the hysteresis loop traces over itself, while maintaining the same area (and therefore dissipation) within the loop. The existence of hysteresis even after creep has stopped under quasistatic perturbation implies: (a) the friction coefficient alone controls the area within the hysteresis curve; (b) to our best knowledge, the hysteresis does not vanish at a finite, yet infinitesimal $\Delta\phi$; and (c) as we show below, both μ and $\Delta\phi$ control the "quasistatic creep rate."

Given the uncertainty in the effect of parasitic friction, it is difficult to be confident about the functional form of the relaxation. Significant care would be required to tease out these relationships accurately but the qualitative dependence on μ and $\Delta\phi$ seems solid.

V. DISCUSSION

Having presented the results, we now discuss them vis-à-vis ideal granular jamming, explain how they are related to each other, and establish how they are related to prior works. We start with the first compression cycle where fragile behavior is observed. The critical packing fraction ϕ_c in ideal jamming is that packing fraction at which two conditions are simultaneously met: (i) the packing fraction at which pressure starts rising above zero and (ii) the isostatic point where total degrees of freedom equal the total number of constraints, i.e., the number of floppy modes equals $D(D+1)/2$ (rigid body rotation and translation), and all individual disk displacements are strongly impeded. The first condition is met at ϕ_1, the packing fraction at which pressure starts rising above zero (albeit exponentially and not power law). The second condition is met, however, only at ϕ_2 where all displacements become very small; ergo the two conditions defining ϕ_c are well separated by a fragile, exponential regime characterized by simultaneous existence of nonzero pressure (jammed clusters) and nonzero displacements (unjammed clusters). As noted in Sec. II A, however, the definition of a contact in ideal jamming permits the system exist in any one of two discrete states, completely unjammed or completely jammed; an intermediate regime as demonstrated by the fragile state is not allowed. This anomalous behavior therefore raises several questions vis-à-vis the ideal jamming paradigm, which we explain below.

(i) Why have prior studies that have successfully verified the jamming predictions not reported this anomalous scaling behavior? All prior experimental [5,33] and numerical [2] studies to our knowledge study the unjamming transition, i.e., they approach ϕ_c from the jammed state towards the unjammed state. An analysis of the unjamming over jamming transition is favored for technical reasons. Precise detection of pressure rise commencement around ϕ_c is very difficult to detect over numerical or instrumental noise and fluctuations from discrete configurational adjustments during compression. We, therefore, believe the fragile state exists in their systems but forms part of the experimental preparation phase, which may not have been systematically analyzed.

Two exceptions lend support to this possibility. In recent numerical work on contact percolation transition (CPT), Shen *et al.* [17] analyzed the approach to jamming transition and show deviations (discussed below) occur prior to jamming onset. But perhaps of greater relevance to the present study is the earlier experimental work of X. Cheng [11] where the jamming transition was studied by swelling tapioca pearls in water. Of particular interest is Fig. 14 of Ref. [11] where the structural factor (pair correlation), measured boundary force, and mean-square particle displacements are plotted against packing fraction. The force exhibits two distinct regimes at packing fractions labeled ϕ_1 and ϕ_2, where ϕ_2 is shown to coincide with random close packing. The pair correlation function exhibits two distinct peaks at ϕ_1 and ϕ_2. Finally, the mean-square displacement goes through a maximum between ϕ_1 and ϕ_2 and falls to zero at ϕ_2. This behavior is related to existence of local jammed clusters starting at ϕ_1 which grow until global jamming is achieved at ϕ_2. That study traces the source of this anomalous behavior to friction, the proof in support being vibrational disturbances (nonzero granular temperature) relieve these frictional contacts and recover ideal jamming predictions (see Fig. 16 in Ref. [11] and related discussion). Given frictional jamming exhibits sensitive dependence on experimental protocol and preparation history, the correspondence between Cheng's experiment and the present study is noteworthy, particularly since they follow different experimental protocols.

(ii) Does an alternative physical mechanism explain the fragile state? In the fragile regime, part of the system is jammed as evidenced by nonzero pressure [Fig. 4(b)], while the remainder is unjammed as evidenced by nonzero displacements (Fig. 5). The co-incidence of exponential pressure rise and fall in displacements with increasing ϕ points to the percolation of jammed clusters across the system. Evidence of stress percolation comes in two parts: first, the strong spatial correlation between local disk displacements and nucleation of new stressed contacts [Figs. 5(c) and 6] and, second, exponential decrease in the fractional area enclosed by stress chains (Fig. 7). The present work is not isolated in its claim of a percolation route to jamming. Several recent studies [12,13,17] have shown some form of percolation mechanism preceding the jamming transition.

(iii) How does friction control the fragile state? Figure 2 presents clear evidence that the start of fragile state (or ϕ_1) is directly dependent on the friction coefficient. With increasing value of the friction coefficient, the fragile state commences at a lower packing fraction. In Fig. 12 we replot the data presented in Fig. 2 on a log-linear scale for PE, PEG, and PEA disks. The data for PEG and PEA are horizontally shifted so their ϕ_1 values coincide with that of PE disks. It is apparent from Fig. 12 that PE and PEG disks have the same exponential slope ($P \propto e^{\phi/\chi_P}$, $\chi_P = 0.00195$). They share the same modulus ($E = 2.5$ GPa) but different friction coefficients

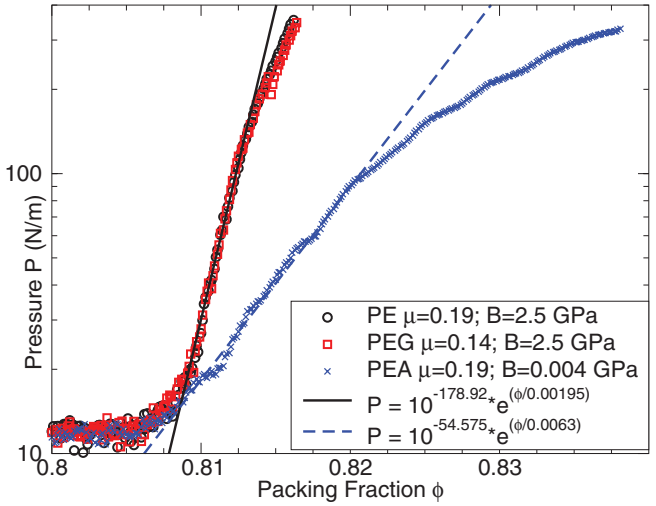

FIG. 12. (Color online) P vs ϕ in log-linear scale for the first compression cycle. All plots have been horizontally shifted for coincidence of ϕ_1. The exponential pressure scaling ($P \propto e^{\phi/\chi_P}$) for PE and PEG exhibits same slope ($\chi_P = 0.00195$) as demonstrated by the exponential fit (solid black line), implying variation in friction coefficient has no effect on χ_P. On the other hand, PEA disks with same friction coefficient as PE, but lower modulus exhibit a shallower exponential scaling (with $\chi_P = 0.0063$, long dashed blue line) over approximately same range of pressure as PE and PEG.

($\mu = 0.19$ for PE $\mu = 0.14$ for PEG), suggesting friction has no measurable effect on the slope of exponential pressure scaling. In contrast, the fragile regime for PEA disks which have same friction coefficient as PE disks ($\mu = 0.19$) but have much lower modulus ($E = 0.004$ GPa) show shallower scaling with $\chi_P = 0.0063$, implying χ_P depends on the modulus. The values of χ_P for all materials are provided in Table II.

The above results do not mean, however, that friction has no effect on χ_P. Frictionless disks (ideal jamming conditions) under compression only jam under normal stresses. Any tangential stress would cause them to slip and disturb local jammed clusters. Therefore, nonzero friction is an essential component for the metastability of the fragile state, even though it does not reveal itself in the preceding discussion, because there are two modulii entering the pressure measurement, the modulus of the disk material and the effective pack modulus. We have only varied the disk material modulus; the pack modulus, on the other hand, is a function of coordination number, which in turn depends on the friction coefficient. Hence, the effective pack modulus is nonlinear due to coordination number; a fact

TABLE II. Experimentally determined values of the exponential slope χ_P for indicated materials (abbreviations defined in text).

Material	ϕ_1	μ	E (GPa)	Exponential slope χ_P
PE	0.8093	0.19	2.5	0.00195
PEG	0.8131	0.14	2.5	0.00195
PEA	0.8079	0.19	0.004	0.0063
LEX	0.7778	0.22	2.0	0.00135
TEF	0.8298	0.06	0.5	0.0021

also evident from power-law scaling of P versus ϕ curves, equivalent to stress-strain relations, in ideal jamming. From that relation [$P \propto (\phi - \phi_c)^{\psi}$] one can discern the nonlinear effective modulus must be $\psi - 1$. We note two subtleties that arise here. First, all experimental, and most numerical, P versus ϕ curves are measured for finite systems, and the asymptotic approach of ψ in the thermodynamic limit (large system size) is not understood. This would be the ideal limit at which to study the nonlinear elastic constants. Albeit subtle, nonlinear elastic constants play a central role in elastoplastic responses of amorphous solids [34,35]. Further, since the Coulomb yield criterion ($F_T \leqslant \mu F_N$) provides only a lower bound on the value of the tangential stress component, it is not possible to experimentally or theoretically learn how friction controls the coordination number and, therefore, the effective pack modulus. Empirical deduction from numerical simulations may be able to shed some light on this relationship but, at this point, one can only say that friction controls the exponential slope χ_P indirectly via effective pack modulus.

(iv) Why is fragile behavior not observed during subsequent compression cycles? When we decompress the system after the first compression cycle, the stresses in the pack are relieved and the boundaries move just enough to relax the system. The disks, however, are left in the final configuration in which they found themselves at the end of the first compression cycle. If the granular pack is subjected to a second compression, the contacts that existed at end of the first compression cycle are immediately activated everywhere across the system simultaneously at a critical packing fraction ϕ_c. This situation exactly corresponds to the sudden system wide emergence of stressed contacts at ϕ_c.

In Fig. 13, we plot the pressure P against the packing fraction ϕ for the second compression cycle. We recall that jamming theory predicts zero pressure below ϕ_c. At ϕ_c when the system satisfies the isostatic condition, and all constraints are activated simultaneously across the system, a rise in pressure is recorded with a power-law scaling [$P \propto (\phi - \phi_c)^{\psi}$]. Prior experiments by Majmudar *et al.* [5] have demonstrated the power-law increase in pressure with an exponent of 1.1. Our experimental data are fit very well with an exponent of 1.15 (see solid line fit for the experimental data in Fig. 13) and are in very good agreement with the results in Ref. [5]. Given that Majmudar *et al.* tapped their system after each quasistatic step, which we do not, the agreement in the exponent is indeed remarkable.

The incompatibility between zero friction and zero temperature raises another important question about what it means for a frictional granular pack to be structurally stable. As argued in Ref. [7], with increasing friction a granular pack can jam at $\phi_c < \phi_{\mathrm{RCP}}$, and the isostatic point can occur at $D + 1 \leqslant Z_c \leqslant 2D$. At zero temperature but nonzero friction, repetitive loading data (Fig. 11) exhibit evolution in ϕ_c, implying there must be an increase in Z_c at each cycle which we are unable to measure due to experimental shortcomings. Nevertheless, a straightforward physical interpretation for hysteretic creep may be presented from the granular jamming perspective. Due to friction, the system jams at ϕ_c into a metastable configuration and will remain so indefinitely unless perturbed externally (recall, the disks are macroscopic and

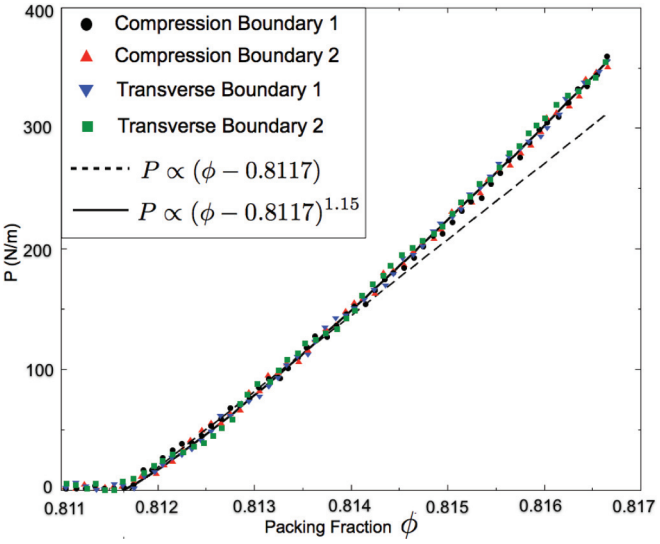

FIG. 13. (Color online) P vs ϕ for the second compression cycle in linear scale shows the predicted power law scaling for granular jamming transition for all four boundaries. The pressure rise is abrupt and is in contrast with the gradual (exponential) rise observed for the first compression cycle. The solid line is the best power-law fit to the experimental data with a power law exponent of 1.15. The long-dashed line representing the best linear fit to the data demonstrates that the experimental data does not follow linear scaling.

not susceptible to thermal fluctuations). Any external driving (e.g., tapping or jiggling) relieves frictional stresses in the system (at least partially if not all of them) and destroys this metastable configuration. In the absence of such external drive, the only perturbative mechanism available to the system is the magnitude of the quasistatic step ($\Delta\phi$) which is equivalent to strain. Hence, it follows that with each loading-unloading cycle, the system evolves ever so slightly through a series of metastable configurations towards a final, stable configuration. The magnitude of $\Delta\phi$ therefore directly controls the pack evolution as shown in the bottom panel of Fig. 11. Furthermore, whether or not a given value of $\Delta\phi$ can evolve the system from one metastable configuration to the next depends on the static friction coefficient μ which controls the degree of a configuration's stability—the higher the friction coefficient, the more stable a configuration is. The rate at which ϕ_c evolves therefore must be a function of μ and $\Delta\phi$. Indeed, as shown in Fig. 11, the difference $(\phi_c^n - \phi_c^0)$ between ϕ_c for the n^{th} and 0^{th} cycles depends on $\Delta\phi$ and μ.

Interestingly, strain-dependent creep and hysteresis are also observed in viscoelastic materials, which represent an entirely different class of amorphous media. Viscoelastic media (unlike purely elastic materials) are characterized by the presence of both an elastic and viscous component. For this reason, whereas purely elastic materials dissipate no energy on application and subsequent removal of a load (reversible process), a viscoelastic medium does dissipate energy via viscosity (irreversible process) [21]. This is seen through the presence of hysteresis in the stress-strain curve, with the area under the hysteresis loop being equal to the energy lost during the loading cycle. Viscosity being resistance to thermally activated plastic deformation, viscous and viscoelastic media lose energy through a loading cycle, i.e., plastic deformation results in energy dissipation, a property uncharacteristic of a purely elastic material's reaction to a loading cycle.

More specifically, viscoelasticity is a molecular rearrangement. Application of stress to a viscoelastic material, e.g., a polymer, cause parts of the long polymer chain to change their positions. This rearrangement is termed *viscoelastic creep* [36]. Polymers retain their solid properties, even as parts of their chains undergo rearrangement in order to accompany the stress, and as this occurs, it creates a back stress in the material. When the magnitude of back stress equals that of the the applied stress, the material ceases to exhibit creep. Unlike viscoelastic media where creep and healing of metastable polymer configurations are thermally activated, in the athermal granular system considered here, the quasistatic strain is the only perturbative mechanism available by which the system creeps towards its ultimate stable configuration at ϕ_{RCP}. Whereas the dissipative mechanism available to viscoelastic amorphous media is supplied by viscosity, in the granular system it comes about through friction. Such viscoelastic behavior has been observed in naturally occurring granular packs in the geophysical context, namely sandstone and sedimentary rocks [15,20]. Particularly noteworthy is that our loading protocol is very similar to loading procedures followed in measuring mechanical properties of geophysical rock samples in standard load cells.

VI. SUMMARY

In summary, we have presented experimental results for a system of bidispersed, frictional disks subjected to uniaxial compression. We verify the numerical predictions for frictional jamming [7,16], whereby jamming is shown to occur at progressively lower packing fractions with increasing friction coefficient. We also show the first compression cycle exhibits exponential increase in pressure and a corresponding exponential fall in displacements over a range of packing fractions $\phi_1 < \phi < \phi_2$. We show this exponential scaling separates the two conditions that define the critical packing fraction ϕ_c. We compare our data against published experimental and numerical results and delve into how friction controls this regime in a nontrivial manner. To put our work in perspective, it falls within a class of recent results that demonstrate some form of percolation mechanism arising prior to jamming transition, with stress percolation presenting the route to jamming in the present case. Finally, we find hysteretic creep under repetitive loading-unloading cycles and experimentally trace its source to friction. Despite our inability to reliably measure coordination numbers, our experiments help explain the various regimes arising in frictional granular jamming.

In conclusion, this article shows jamming in the presence of friction demonstrates rich behavior beyond the ideal jamming scenario. Several subtle, yet important questions arise, as discussed throughout this article. Some of them lie beyond experimental purview where numerical simulations can lend crucial support. Resolution of these questions should aid in development of a tractable theory of frictional jamming, in turn, aiding advances in both fundamental (statistical and condensed matter physics) and applied (materials physics and geophysics) realms alike.

ACKNOWLEDGMENTS

This work was carried out under the auspices of the National Nuclear Security Administration of the US Department of Energy at Los Alamos National Laboratory under Contract No. DE-AC52-06NA25396. The authors gratefully acknowledge helpful discussions with O. Dauchot.

[1] A. J. Liu and S. R. Nagel, Nature **396**, 21 (1998).
[2] C. S. O'Hern, L. E. Silbert, A. J. Liu, and S. R. Nagel, Phys. Rev. E **68**, 011306 (2003).
[3] S. Henkes and B. Chakraborty, Phys. Rev. Lett. **95**, 198002 (2005).
[4] H. Jacquin, L. Berthier, and F. Zamponi, Phys. Rev. Lett. **106**, 135702 (2011).
[5] T. S. Majmudar, M. Sperl, S. Luding, and R. P. Behringer, Phys. Rev. Lett. **98**, 058001 (2007).
[6] F. Radjai, M. Jean, J.-J. Moreau, and S. Roux, Phys. Rev. Lett. **77**, 274 (1996).
[7] L. E. Silbert, D. Ertas, G. S. Grest, T. C. Halsey, and D. Levine, Phys. Rev. E **65**, 031304 (2002).
[8] E. Somfai, M. van Hecke, W. G. Ellenbroek, K. Shundyak, and W. van Saarloos, Phys. Rev. E **75**, 020301(R) (2007).
[9] K. Shundyak, M. van Hecke, and W. van Saarloos, Phys. Rev. E **75**, 010301(R) (2007).
[10] C. Song, P. Wang, and H. A. Makse, Nature **453**, 629 (2008).
[11] X. Cheng, Phys. Rev. E **81**, 031301 (2010).
[12] D. Bi, J. Zhang, B. Chakraborty, and R. P. Behringer, Nature **480**, 355 (2011).
[13] C. Coulais, R. P. Behringer, and O. Dauchot, Europhys. Lett. **100**, 44005 (2012).
[14] D. J. Cumberland and R. J. Crawford, *The Packing of Particles* (Elsevier Science, New York, 1987).
[15] A. N. Tutuncu, A. L. Podio, and M. M. Sharma, Geophysics **63**, 195 (1998).
[16] L. E. Silbert, Softmatter **6**, 2918 (2010).
[17] T. Shen, C. S. O'Hern, and M. D. Shattuck, Phys. Rev. E **85**, 011308 (2012).
[18] C. A. Angell, J. Phys. Chem. Solids. **49**, 863 (1988).
[19] T. A. Vilgis, Phys. Rev. B **47**, 2882 (1993).
[20] K. E. Claytor, J. R. Koby, and J. A. Tencate, Geophys. Res. Lett. **36**, L06304 (2009).
[21] M. A. Meyers and K. K. Chawla, *Mechanical Behavior of Materials* (Cambridge University Press, Cambridge, UK, 2008).
[22] J. D. Bernal, Nature **185**, 68 (1960).
[23] J. D. Bernal and J. Mason, Nature **188**, 910 (1960).
[24] G. D. Scott, Nature **188**, 908 (1960).
[25] S. Torquato, T. M. Truskett, and P. G. Debenedetti, Phys. Rev. Lett. **84**, 2064 (2000).
[26] P. Chaudhuri, L. Berthier, and S. Sastry, Phys. Rev. Lett. **104**, 165701 (2010).
[27] F. Krzakala and J. Kurchan, Phys. Rev. E **76**, 021122 (2007).
[28] S. Inagaki, M. Otuski, and S.-I. Sasa, Euro. Phys. J. E **34**, 124 (2011).
[29] N. C. Keim and S. R. Nagel, Phys. Rev. Lett. **107**, 010603 (2011).
[30] P. G. Debenedetti, *Metastable Liquids* (Princeton University Press, 1996).
[31] S. Sastry, P. G. Debenedetti, and F. H. Stillinger, Nature **393**, 554 (1998).
[32] J. Zhang, T. S. Majmudar, A. Tordesillas, and R. P. Behringer, Gran. Matter **12**, 159 (2010).
[33] H. P. Zhang and H. A. Makse, Phys. Rev. E **72**, 011301 (2005).
[34] S. Karmakar, E. Lerner, and I. Procaccia, Phys. Rev. E **82**, 026105 (2010).
[35] H. G. E. Hentschel, S. Karmakar, E. Lerner, and I. Procaccia, Phys. Rev. E **83**, 061101 (2011).
[36] J. D. Ferry, *Viscoelastic Properties of Polymers* (John Wiley & Sons, New York, 1980).